A Transmission-Line-Based Decoupling Method for MIMO Antenna Arrays

Zhang, Yiming; Zhang, Shuai; Li, Jia-Lin; Pedersen, Gert F.

Published in:
IEEE Transactions on Antennas and Propagation

DOI (link to publication from Publisher):
10.1109/TAP.2019.2900406

Publication date:
2019

Document Version
Accepted author manuscript, peer reviewed version

This article has been accepted for publication in a future issue of this journal, but has not been fully edited. Content may change prior to final publication. Citation information: DOI 10.1109/TAP.2019.2900406, IEEE Transactions on Antennas and Propagation

A Transmission-Line-Based Decoupling Method for MIMO Antenna Arrays

Yi-Ming Zhang, *Student Member, IEEE*, Shuai Zhang, *Senior Member, IEEE*, Jia-Lin Li, and Gert Frølund Pedersen, *Senior Member, IEEE*

***Abstract*—A transmission-line-based decoupling technique for dual-polarized multiple-input and multiple-output (MIMO) antenna arrays is presented and analyzed. The proposed scheme enables well-canceled coupling for the adjacent elements under co-polarization, without degrading the isolation of the cross-polarized ports. Firstly, a decoupling network based on the presented method for a 2×2 MIMO array is provided, along with a comprehensive design procedure. Calculations and simulations are operated to verify the decoupling performance. For further verification, a 2×2 dual-polarized patch array with the proposed decoupling method is developed. The decoupling network characterizes low profile, compact size, and low insertion loss, which is realized in a single layer. Measurements denote that the isolations between the co-polarized elements are improved from 16-20 dB to over 30 dB after decoupling at the center frequency of 2.45 GHz. Subsequently, based on the proposed 2×2 decoupling method, a decoupling network for large-scale dual-polarized MIMO arrays is presented. A design example of a 4×4 dual-polarized patch antenna array is established. Full-wave simulations indicate that the isolations are enhanced to better than 30 dB with a small insertion loss of less than 0.45 dB, and can widely be used for phased array and massive MIMO array systems.**

***Index Terms*—Multi-input and multi-output (MIMO), phased antenna array, isolation, mutual coupling, dual-polarization.**

I. Introduction

SEEING that the multiple-input and multiple-output (MIMO) systems are powerful to increase the channel capacity and enhance the spectrum efficiency for wireless communications, the studies on MIMO antennas have attracted growing interests. To maintain the active impedance matching performance of MIMO antennas, one challenge is the coupling suppression among antenna elements. Otherwise, the coupling may lead to dramatic degradations of adaptive array whose pattern is adjusted automatically to signal environment [1], significant drops of the mean capacity of a MIMO system [2] as well as other negative effects [3-5]. Although mutual coupling below −17 dB is sufficient for MIMO-based transmission from the error rate point of view [6], such an isolation level does not mean that MIMO capacity can be achieved in practice. For instance, the active VSWR would be higher than six with the isolation of 15 dB [3], which can be highly improved if the mutual coupling is reduced to lower than −25 dB [4]. Besides, nonlinear effects would be caused by the strong coupling in the massive MIMO systems [7]. This would lead to significant nonlinear distortions on power amplifiers, and decrease the operation bandwidth of the systems. To this end, the mutual coupling between the elements of massive MIMO arrays is preferred to be less than −25 dB or even lower in practice.

To suppress the coupling, a great amount of designs have been presented by restraining the surface currents between antennas, such as electromagnetic-bandgap structure [8] and defected ground structure [9], at the cost of specified antenna configurations or large element distances. Using decoupling circuits that are integrated with the feeding network and independent of antenna elements is an attractive way to suppress/cancel the mutual coupling since antenna structures and element distances would not be the issues theoretically [10]-[18]. For compactness, utilizing lumped decoupling technologies is an effective technique. In [10]-[12], *LC*-based architectures were proposed for closely coupled dual-element arrays. Despite the achieved inter-port isolation, degradation of efficiency was observed owing to the parasitic effects of the introduced *LC* components. On the other hand, transmission-line-based decoupling methods, e.g. in [13]-[18], become more attractive for their low profile and high efficiency (due to the lower insertion loss) compared with those *LC* circuits. For instance, in [18], a microstrip-line-based decoupling network was studied and designed for asymmetrical dual-element arrays with the measured efficiency of over 90% at the studied frequencies.

Most of the approaches mentioned above focus on the decoupling for dual-element arrays. Mutual coupling suppression for antenna arrays with more than two elements is still a challenge, especially for dual-polarized arrays. Several efforts have been devoted to enhancing the isolation for such arrays [19]-[26]. For instance, decoupling networks for linear arrays with single linear polarization were studied and designed in [19] and [20]. In [21] and [22], decoupling networks for miniaturized antenna arrays consisting of three and four antenna elements were studied, respectively. Theoretical analyses verified the decoupling performance, but without any

This work was supported by the China Scholarship Council, and also partially supported by AAU Young Talent Program. (*Corresponding author*: *Shuai Zhang*.)

Yi-Ming Zhang and Jia-Lin Li are with the School of Physics, University of Electronic Science and Technology of China, Chengdu 610054, China. Yi-Ming Zhang is also with the Antenna, Propagation and Millimeter-wave Systems (APMS) Section, Aalborg University, Aalborg 9220, Denmark (e-mail: ymzhang@std.uestc.edu.cn, yiming@es.aau.dk, jialinli@uestc.edu.cn).

Shuai Zhang and Gert Frølund Pedersen are with the Antenna, Propagation and Millimeter-wave Systems (APMS) Section, Aalborg University, Aalborg 9220, Denmark (e-mail: sz@es.aau.dk, gfp@es.aau.dk).

This article has been accepted for publication in a future issue of this journal, but has not been fully edited. Content may change prior to final publication. Citation information: DOI 10.1109/TAP.2019.2900406, IEEE Transactions on Antennas and Propagation

practical examples. Besides, the realization for dual-polarized arrays and especially for the massive MIMO arrays was also an issue due to the complicated network configurations. In [23] and [24], decoupling methods were proposed for 2×2 arrays with single linear polarization. In [23], four 90-degree branch-line couplers based on microstrip transmission lines were applied to reduce the coupling. However, the decoupling method significantly changes the radiation patterns of antenna elements. Since both the array configuration and the excitations should be under specified requirements, the network is also very difficult for the use of dual-polarized MIMO arrays. Reactively loaded dummy elements were placed in the central area of a 2×2 array for isolation enhancement [24]. This technique is effective but not suitable for dual-polarized 2×2 arrays, since dummy elements have to be dual-polarized and small enough to fit the very crowded inter-element space. In [25], a dual-polarized massive MIMO array featuring high inter-port isolation of over 25 dB was presented, at the cost of bulky system and specified antenna type. More recently, the concept of the array decoupling surface was introduced in [26]. By placing a surface consisting of metal patches in front of antenna arrays, additional reflections were constructed to cancel the mutual coupling of a 2×2 dual-polarized array. However, the surface was typically placed around quarter-wavelength away from an array in order to not alter the antenna radiation performance and achieve good isolation, which made antenna systems bulky.

In this work, a transmission-line-based decoupling technique is presented and analyzed to cancel the mutual coupling within dual-polarized MIMO antenna arrays. A complete design procedure of the network is formulated and explicated for realization purposes. Compared with the existing decoupling methods, the proposed scheme features more efficient decoupling for dual-polarized arrays with simple structures, low profile, and low insertion loss. The specified contributions and novelties of this work are as follows:

(1) For 2×2 dual-polarized antenna arrays, a two-order decoupling network is proposed to cancel the three kinds of the couplings (between the vertical, horizontal and diagonal pairs of elements) among the co-polarized ports, with no deterioration in the isolation of the cross-polarized ports. The developed decoupling network can be realized in a single substrate layer, which is verified by both the full-wave simulated and measured results;

(2) By employing the proposed 2×2 decoupling network as the grid cell, a lattice decoupling architecture for large-scale arrays is further established. To our knowledge, this is the first time that transmission-line-based decoupling network is presented for the massive arrays with dual-polarization operation. The adjacent co-polarized ports are well decoupled with no degradation in the isolation between non-adjacent ports. The isolation between cross-polarized ports are kept in high level or even improved. 3D full-wave simulations are carried out to verify the performance. The proposed network is operated within two substrate layers, and can be easily integrated and miniaturized using low-profile multilayer manufacturings, such as multilayer PCB technique.

This paper is organized as follows. Section II provides the detailed analysis and the summarized design procedure of the proposed decoupling method for 2×2 arrays. In Section III, design descriptions and numerical investigations based on Section II for a detailed 2×2 dual-polarized patch antenna array are presented. The measured results followed by the full-wave simulated results are given in Section IV. Section V provides the analysis of the decoupling network for large-scale arrays based on the proposed 2×2 decoupling network. A design example of a 4×4 dual-polarized patch array is also given in Section V. Conclusions are finally stated in Section VI.

II. Proposed Decoupling Network for 2×2 Arrays

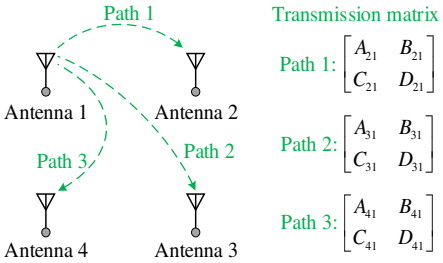

Fig. 1. Mutual couplings between antenna 1 and others within a 2×2 antenna array.

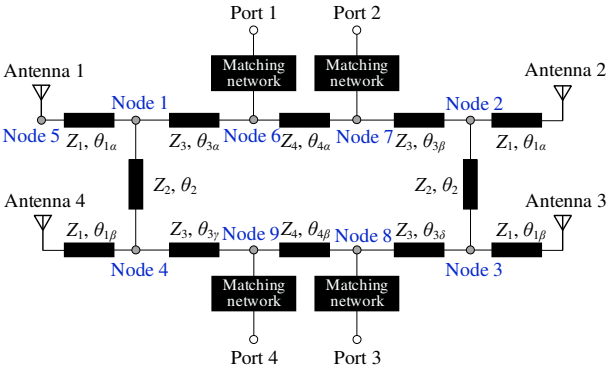

Fig. 2. Block diagram of the proposed decoupling network for 2×2 antenna arrays.

In general, the couplings among cross-polarized elements in dual-polarized antenna arrays are weak enough with no necessity for taking into account the decoupling. On the other hand, during the decoupling between the co-polarized elements, the high isolation between the cross-polarized ports should not be deteriorated. Obviously, this is not a requirement satisfied by all the published decoupling networks, but can be achieved by using the method proposed in this paper. Subsequently, the process of the decoupling for the array can be separated into two similar but independent steps that respectively deal with the couplings of two subarrays classified by polarization. Therefore, the following studies in this section will center on the decoupling network for a 2×2 single-polarized MIMO antenna array. Finally, the decoupling for a 2×2 dual-polarized array can be realized by simply using two independent networks corresponding to the elements with two polarizations, respectively.

Fig. 1 shows the configuration of a generic 2×2 antenna array

This article has been accepted for publication in a future issue of this journal, but has not been fully edited. Content may change prior to final publication. Citation information: DOI 10.1109/TAP.2019.2900406, IEEE Transactions on Antennas and Propagation

including four identical elements marked as antennas 1, 2, 3 and 4. Taking antenna 1 as a case study, the coupling paths between antenna 1 and the other three elements are given in Fig. 1, where the transmission matrices of these paths are also provided. In general, the mentioned matrices would not be identical, leading to a challenge to suppress all the coupling among these antenna elements. To this end, we proposed a ring network for decoupling purposes in 2×2 MIMO antenna arrays, as illustrated in Fig. 2. The presented decoupling network consists of twelve transmission lines with different characteristic impedances and electric lengths. With this network, all the couplings within the 2×2 antenna array can be canceled theoretically. The determinations of the parameters for the proposed network are studied in the following discussions. Note that due to the symmetry configuration as shown in Fig.1, the couplings are classified into three types that will be discussed separately, and antenna 1 is employed as the studied case. It can be readily concluded that all the couplings within the 2×2 antenna array can be well suppressed ideally, on condition that the couplings between antenna 1 and the others are decoupled.

A. *Decoupling of the vertical pair of antenna elements*

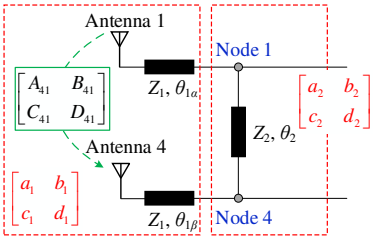

Fig. 3. Simplified circuit for the decoupling between antennas 1 and 4.

Fig. 3 depicts the simplified equivalent circuit for the decoupling between the vertical pair of the antennas, that is, antennas 1 and 4 in this case. For this part, the two antennas are respectively loaded at the end of two transmission lines connected with a transmission-line bridge. The parameters of the transmission lines are defined as marked in Fig. 3. Therefore, the transmission matrices between nodes 1 and 4 through the antenna coupling (a_1, b_1, c_1, d_1) and the transmission-line bridge (a_2, b_2, c_2, d_2) can be calculated based on microwave network theory [27], given as

$$\begin{bmatrix} a_1 & b_1 \\ c_1 & d_1 \end{bmatrix} = \begin{bmatrix} \cos\theta_{1\alpha} & jZ_1\sin\theta_{1\alpha} \\ \dfrac{j\sin\theta_{1\alpha}}{Z_1} & \cos\theta_{1\alpha} \end{bmatrix} \begin{bmatrix} A_{41} & B_{41} \\ C_{41} & D_{41} \end{bmatrix} \begin{bmatrix} \cos\theta_{1\beta} & jZ_1\sin\theta_{1\beta} \\ \dfrac{j\sin\theta_{1\beta}}{Z_1} & \cos\theta_{1\beta} \end{bmatrix} \quad (1)$$

$$\begin{bmatrix} a_2 & b_2 \\ c_2 & d_2 \end{bmatrix} = \begin{bmatrix} \cos\theta_2 & jZ_2\sin\theta_2 \\ \dfrac{j\sin\theta_2}{Z_2} & \cos\theta_2 \end{bmatrix}. \quad (2)$$

where $[A_{41}\ B_{41};\ C_{41}\ D_{41}]$ is the equivalent transmission matrix of the coupling between the two elements; Z_1, Z_2, $\theta_{1\alpha}$, $\theta_{1\beta}$, and θ_2 are the parameters of the transmission lines, as shown in Fig. 2. Based on (1) and (2), the mutual admittance from node 1 to node 4 can be expressed as

$$Y_{41} = -\frac{1}{b_1} - \frac{1}{b_2} \quad (3a)$$

$$b_1 = jA_{41}Z_1\cos\theta_{1\alpha}\sin\theta_{1\beta} + jD_{41}Z_1\sin\theta_{1\alpha}\cos\theta_{1\beta} + B_{41}\cos\theta_{1\alpha}\cos\theta_{1\beta} - C_{41}Z_1^2\sin\theta_{1\alpha}\sin\theta_{1\beta} \quad (3b)$$

$$b_2 = jZ_2\sin\theta_2. \quad (3c)$$

For decoupling between nodes 1 and 4, we have

$$Y_{41} = 0. \quad (4)$$

According to (4), the following design requirements can be derived

$$\theta_{1\alpha} = \arctan\left(\frac{\mathrm{Re}[B_{41}] - \mathrm{Im}[A_{41}]Z_1\tan\theta_{1\beta}}{\mathrm{Re}[C_{41}]Z_1^2\tan\theta_{1\beta} + \mathrm{Im}[D_{41}]Z_1}\right) \quad (5)$$

$$\frac{1}{Z_2\sin\theta_2} = \mathrm{Im}\left[\frac{1}{b_1}\right]. \quad (6)$$

One can observe from (5) that for arbitrarily given values of Z_1 and $\theta_{1\beta}$, the solution for $\theta_{1\alpha}$ always exists. Furthermore, combining (5) with (6), it is seen that for the given values of Z_1, $\theta_{1\beta}$, and $\theta_{1\alpha}$, there would have at least one solution for ($Z_2\sin\theta_2$). The analysis implies that the coupling between antennas 1 and 4 can be canceled by using the design descriptions shown in (3)-(6). Note that the impedance matching performance is not necessary to be studied for nodes 1 and 4 in this part, since they can be achieved at the final input interfaces of the decoupling network as shown in Fig. 2, which will be mentioned later in this paper.

B. *Decoupling of the diagonal pair of antenna elements*

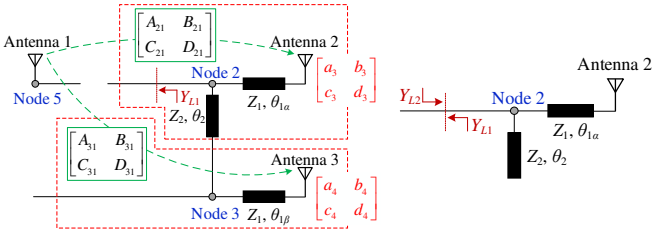

Fig. 4. (a) Suppression network for the coupling between antennas 1 and 3. (b) Simplified equivalent circuit for the derivation of the parameter Y_{L1}.

As for the coupling between diagonally positioned antennas 1 and 3, its suppression network is shown in Fig. 4(a). It is found that input power at node 5 provided for antenna 1 would partially flow to the node 3 through two paths corresponding to the couplings between antennas 1 and 2, and antennas 1 and 3, respectively. Then, the transmission parameters of the two paths can be obtained, as given by

$$\begin{bmatrix} a_3 & b_3 \\ c_3 & d_3 \end{bmatrix} = \begin{bmatrix} A_{S1} & B_{S1} \\ C_{S1} & D_{S1} \end{bmatrix} \begin{bmatrix} \cos\theta_2 & jZ_2\sin\theta_2 \\ \dfrac{j\sin\theta_2}{Z_2} & \cos\theta_2 \end{bmatrix} \quad (7)$$

$$\begin{bmatrix} a_4 & b_4 \\ c_4 & d_4 \end{bmatrix} = \begin{bmatrix} A_{31} & B_{31} \\ C_{31} & D_{31} \end{bmatrix} \begin{bmatrix} \cos\theta_{1\beta} & jZ_1\sin\theta_{1\beta} \\ \dfrac{j\sin\theta_{1\beta}}{Z_1} & \cos\theta_{1\beta} \end{bmatrix} \quad (8)$$

where

$$\begin{bmatrix} A_{S1} & B_{S1} \\ C_{S1} & D_{S1} \end{bmatrix} = \begin{bmatrix} A_{21} & B_{21} \\ C_{21} & D_{21} \end{bmatrix} \begin{bmatrix} \cos\theta_{1\alpha} & jZ_1\sin\theta_{1\alpha} \\ \dfrac{j\sin\theta_{1\alpha}}{Z_1} & \cos\theta_{1\alpha} \end{bmatrix} \begin{bmatrix} 1 & 0 \\ Y_{L1} & 1 \end{bmatrix} \quad (9a)$$

This article has been accepted for publication in a future issue of this journal, but has not been fully edited. Content may change prior to final publication. Citation information: DOI 10.1109/TAP.2019.2900406, IEEE Transactions on Antennas and Propagation

$$A_{S1} = A_{21}\cos\theta_{1\alpha} + \frac{jB_{21}\sin\theta_{1\alpha}}{Z_1} + Y_{L1}\left(jA_{21}Z_1\sin\theta_{1\alpha} + B_{21}\cos\theta_{1\alpha}\right) \quad (9b)$$

$$B_{S1} = jA_{21}Z_1\sin\theta_{1\alpha} + B_{21}\cos\theta_{1\alpha}\,. \quad (9c)$$

where $[A_{21}\ B_{21};\ C_{21}\ D_{21}]$ and $[A_{31}\ B_{31};\ C_{31}\ D_{31}]$ are the equivalent transmission matrices of the couplings between elements 1 and 2, elements 1 and 3, respectively. Then we can obtain the mutual admittance from node 5 to node 3 through the two leakage paths, expressed as

$$Y_{31} = -\frac{1}{b_3} - \frac{1}{b_4}\,. \quad (10)$$

In order to suppress the two couplings, we have

$$Y_{31} = 0\,. \quad (11)$$

The following expression can then be derived based on (11)

$$jA_{31}Z_1\sin\theta_{1\beta} + B_{31}\cos\theta_{1\beta} + jA_{S1}Z_2\sin\theta_2 + B_{S1}\cos\theta_2 = 0\,. \quad (12)$$

The parameter Y_{L1} described in (9) denotes the admittance looking toward the input interface at node 2. Seeing that for the entire network proposed in Fig. 2, impedance matching would be realized finally, and thus the value of Y_{L1} would equal to the admittance Y_{L2} looking toward the antenna 2 at node 2. Then, the admittance Y_{L1} can be considered as a function of Z_2 and θ_2, when the values of Z_1, $\theta_{1\beta}$, and $\theta_{1\alpha}$ are selected based on (5). Furthermore, according to (11), node 3 can be treated as an open node when antenna 2 is excited, and the corresponding equivalent circuit is shown in Fig. 4(b). Subsequently, we have

$$Y_{L1} = Y_{L2} = \frac{Z_1 + jZ_{AN}\tan\theta_{1\alpha}}{Z_1(Z_{AN} + jZ_1\tan\theta_{1\alpha})} + \frac{j\tan\theta_2}{Z_1} \quad (13)$$

where Z_{AN} is the input impedance of the antenna element. As a result, (12) is a function of Z_2 and θ_2 on the condition of (5). On the basis of the above discussions, one can find that with the design requirements described in (3)-(6) and (12), couplings between the pairs of both vertical and diagonal antennas would be well canceled. Note that the decoupling between antennas 1 and 2 is not carried out in this part, which will be achieved in the coming discussion.

C. *Decoupling of the horizontal pair of antenna elements*

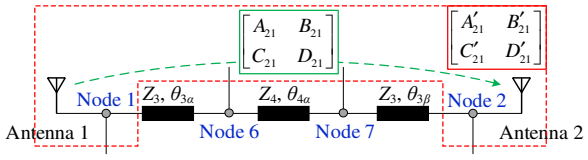

Fig. 5. Cancellation circuit for the coupling between antennas 1 and 2.

Fig. 5 shows the cancellation network for the coupling between the horizontal pair of antennas (antennas 1 and 2). The path from the node 1 to node 2 through the coupling between antennas 1 and 2 can be considered as a combined signal flow with a combined transmission matrix, as defined and depicted in the upper right corner of Fig. 5. Assuming that the parameters Z_1, $\theta_{1\beta}$, $\theta_{1\alpha}$, Z_2, and θ_2 are already determined according to the above studies, the combined transmission parameters (A'_{21}, B'_{21}, C'_{21}, and D'_{21}) can be calculated. Hence, following the discussions in Section II-A, by referring to the similar derivations for the achievements of (5)-(7), the values of Z_3, $\theta_{3\alpha}$, $\theta_{3\beta}$, Z_4, and $\theta_{4\alpha}$ can be determined, expressed as

$$\theta_{3\alpha} = \arctan\left(\frac{\mathrm{Re}[B'_{21}] - \mathrm{Im}[A'_{21}]Z_3\tan\theta_{3\beta}}{\mathrm{Re}[C'_{21}]Z_3^2\tan\theta_{3\beta} + \mathrm{Im}[D'_{21}]Z_3}\right) \quad (14)$$

$$\frac{1}{Z_4\sin\theta_{4\alpha}} = \mathrm{Im}\left[\frac{1}{b'_1}\right] \quad (15)$$

where

$$b'_1 = jA'_{21}Z_3\cos\theta_{3\alpha}\sin\theta_{3\beta} + jD'_{21}Z_3\sin\theta_{3\alpha}\cos\theta_{3\beta} + B'_{21}\cos\theta_{3\alpha}\cos\theta_{3\beta} - C'_{21}Z_3^2\sin\theta_{3\alpha}\sin\theta_{3\beta}\,. \quad (16)$$

Consequently, on the strength of (3)-(6) and (12)-(16), the coupling between antenna 1 and the other three antennas can be well suppressed. For the parameters of $\theta_{3\gamma}$, $\theta_{3\delta}$, and $\theta_{4\beta}$ described in Fig. 2, similar derivations can be adopted to determine the values, and thus are not detailed here for brevity.

D. *Signal flow study of the proposed decoupling network*

In view of the above analyses carried out separately for different coupling paths, an overall study is essential to verify the decoupling performance between the four ports of the proposed network. Here, a case study for the decoupling between port 1 and the other ports is performed by employing a signal flow graphical analysis.

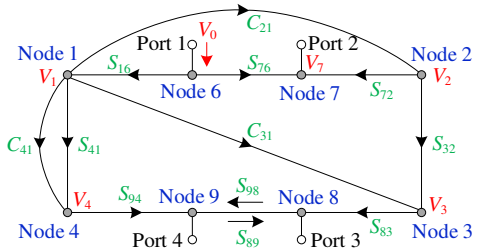

(a)

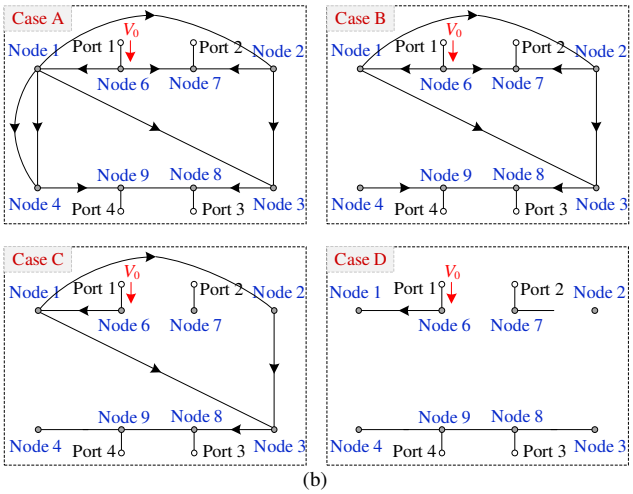

(b)

Fig. 6. (a) Simplified signal flow representation for the decouplings between port 1 and other ports of the proposed network. (b) Graphical evolution of the equivalent signal flow through the network.

Defining that the input voltage at the interface of port 1 is V_0, the voltages at other nodes can be readily derived as illustrated in Fig. 6, where parameters S_{ij} is the transmission coefficient between the nodes, and C_{mn} is the coupling coefficient between the antenna elements. Hence, the voltages at nodes 7, 8, and 9 can be calculated using signal flow decomposition method [27]

This article has been accepted for publication in a future issue of this journal, but has not been fully edited. Content may change prior to final publication. Citation information: DOI 10.1109/TAP.2019.2900406, IEEE Transactions on Antennas and Propagation

$$V_7 = \left(S_{76} + S_{72}C_{21}S_{16}\right)V_0 \tag{17a}$$

$$V_8 = S_{89}S_{94}\left(C_{41}+S_{41}\right)S_{16}V_0 + S_{83}\left(C_{31}+S_{32}C_{21}\right)S_{16}V_0 + S_{83}S_{32}S_{27}S_{76}V_0 \tag{17b}$$

$$V_9 = S_{94}\left(C_{41}+S_{41}\right)S_{16}V_0 + S_{98}S_{83}\left(C_{31}+S_{32}C_{21}\right)S_{16}V_0 + S_{98}S_{83}S_{32}S_{27}S_{76}V_0 . \tag{17c}$$

On the other hand, according to the results derived from Figs. 3, 4, and 5, and the conditions expressed in (4) and (11), we have

$$C_{41} + S_{41} = 0 \tag{18a}$$

$$C_{31} + S_{32}C_{21} = 0 \tag{18b}$$

$$S_{76} + S_{72}C_{21}S_{16} = 0 . \tag{18c}$$

By using (18c) in (17a), it is found the voltage at node 7 is zero. This means that there would no leakage from node 6 to node 7. Then, (17b) and (17c) can be simplified as

$$V_8 = S_{89}S_{94}\left(C_{41}+S_{41}\right)S_{16}V_0 + S_{83}\left(C_{31}+S_{32}C_{21}\right)S_{16}V_0 \tag{19a}$$

$$V_9 = S_{94}\left(C_{41}+S_{41}\right)S_{16}V_0 + S_{98}S_{83}\left(C_{31}+S_{32}C_{21}\right)S_{16}V_0 . \tag{19b}$$

By substituting (18) to (19), one can find that voltages at nodes 8 and 9 are all zero. The results indicate that there would be no signals leaking from port 1 to the other ports ideally. Besides, there would also be no leakage from port 1 to antennas 2, 3, and 4. This can be verified by the graphical evolution of the signal flow through the network, as illustrated in Fig. 6(b). The signal flow of case A shown in Fig. 6(b) corresponds to the network of Fig. 6(a). As discussed above, case A can be simplified to case B since the voltage at node 4 is zero. Seeing that the voltage at node 7 is zero, the equivalent signal flow is further modified to case C, which can be finally simplified to case D in view of (18b). It is seen from case D that there is no signal flowing from port 1 to nodes 2, 3, and 4 through the network. This denotes that when port 1, 2, 3, and 4 are excited separately, antennas 1, 2, 3, or 4 would work correspondingly. As for the matching networks mentioned in Fig. 2, several classical methods such as multisection transformer can be utilized to achieve the purpose.

E. Design procedure of the proposed decoupling network

By employing the proposed network, the coupling within a 2×2 antenna array can be well canceled according to the above studies. Based on the derived functions expressed in (3)-(6) and (12)-(16), all the parameters of the transmission lines shown in Fig. 2 can be theoretically determined, and easily realized in practice by using full-wave simulations. To clarify the achievement of such a decoupling network, a simple design procedure is summarized as shown in Fig. 7 and given by

Step 1) Determining Z_1, $\theta_{1\alpha}$, $\theta_{1\beta}$, Z_2, and θ_2. Based on the specifications (substrate parameters, center frequency f_0, and mutual coupling coefficients within the 2×2 antenna array), achievable values of Z_1, $\theta_{1\beta}$, and $\theta_{1\alpha}$ are calculated using (5). Furthermore, Z_2 and θ_2 can be selected from (6). Notice that all electric lengths refer to f_0;

Step 2) Calculating the value of Y_{L1}. As the study from (9), the admittance Y_{L1} can be calculated with the confirmed values of Z_1, $\theta_{1\beta}$, $\theta_{1\alpha}$, Z_2, and θ_2;

Step 3) Evaluating and checking whether the values of the parameters satisfy (12) or not. If not, a new group of Z_1, $\theta_{1\beta}$, $\theta_{1\alpha}$, Z_2, and θ_2 should be reselected through the steps 1 and 2 until they fit (12). The purpose of this step is to confirm the obtained values of the parameters enabling the decoupling between the diagonal pair of antennas. It can be readily achieved based on the lossless transmission-line model shown in Fig. 2 by using a circuit simulator like Agilent Advance Design System (ADS);

Step 4) Determining the values of the rest of the components shown in Fig. 2. Based on (14)-(16), these values can be obtained;

Step 5) Determining the impedance matching networks for all ports. By analyzing the impedance performance at the interfaces of all ports, the suitable matching method can be employed. Subsequently, all transmission-line parameters are converted to physical parameters on a specified microwave substrate for a practical purpose;

Step 6) Determining the final layout. The layout of the proposed decoupling network can be initially constructed involving the discontinuities, the soldering pads, and considering the compactness as well as avoiding strong couplings between transmission lines. Further, the structure can be numerically evaluated by using EM simulator like Computer Simulation Technology (CST). To finely tune the physical parameters, optimal electric performance can be utilized to verify the final layout.

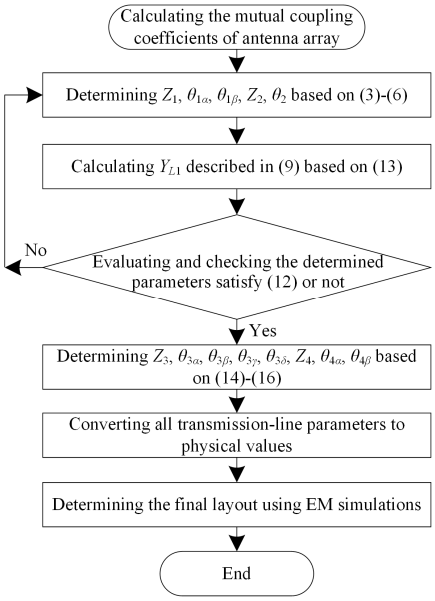

Fig. 7. Design flowchart of the proposed decoupling network for a 2×2 single-polarized antenna array.

In summary, for a 2×2 dual-polarized antenna array, it can be considered as a combination of two 2×2 subarrays with different linear polarization. By utilizing the proposed design procedure to construct two independent decoupling networks for the two subarrays, all the mutual couplings with co-polarization would be canceled. Moreover, there is no deterioration in the isolation between the cross-polarized elements, due to no effects on corresponding coupling paths.

This article has been accepted for publication in a future issue of this journal, but has not been fully edited. Content may change prior to final publication. Citation information: DOI 10.1109/TAP.2019.2900406, IEEE Transactions on Antennas and Propagation

III. Numerical Study of a Typical Example

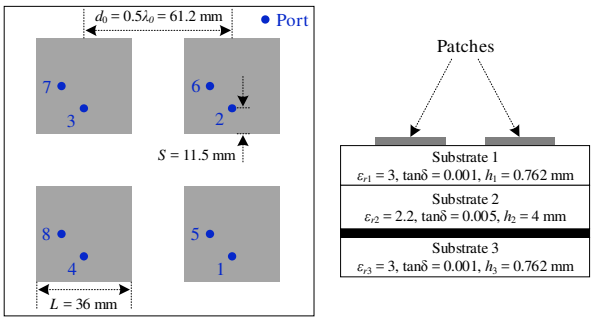

Fig. 8. Geometric structure of the employed microstrip antenna array.

For verification purpose, a typical example centered at 2.45 GHz is presented. More specifically, a 2×2 dual-polarized microstrip antenna array is studied and developed to validate the capability of the proposed decoupling technique. The studied array includes three concentrically stacked substrates and a shared ground plane, as illustrated in Fig. 8. Four microstrip patches are printed on the top of substrate 1, and the ground is inserted between substrates 2 and 3. The center-to-center distance d_0 between two adjacent antenna elements is $0.5\lambda_0$, where λ_0 is the free space wavelength at 2.45 GHz. The decoupling network will be positioned on the bottom of substrate 3. In this section, detailed design descriptions are presented for the array based on numerical investigations. Here, the decoupling for the subarray corresponding to ports 1, 2, 3, and 4 with vertical polarizations is detailed as a case study, as provided below.

A. *Numerical-based graphical study*

Prior to giving the determination of the decoupling network, the coupling response within the array is studied to obtain the required mutual transmission matrices mentioned in Fig. 1. By using EM simulator (CST in this paper), the scattering parameters of the antenna array without decoupling can be readily observed through full-wave simulations. The mutual transmission matrices can be then evaluated, which are

$$\begin{bmatrix} A_{21} & B_{21} \\ C_{21} & D_{21} \end{bmatrix} = \begin{bmatrix} 5.454 - j0.167 & 306.0 + j46.315 \\ 0.0919 - j0.0184 & 5.423 - j0.0699 \end{bmatrix} \quad (20a)$$

$$\begin{bmatrix} A_{31} & B_{31} \\ C_{31} & D_{31} \end{bmatrix} = \begin{bmatrix} -5.779 + j11.132 & -441.58 + j569.89 \\ -0.0675 + j0.2094 & -5.9919 + j11.102 \end{bmatrix} \quad (20b)$$

$$\begin{bmatrix} A_{41} & B_{41} \\ C_{41} & D_{41} \end{bmatrix} = \begin{bmatrix} 2.9604 - j1.8176 & 184.74 - j76.402 \\ 0.0435 - j0.0411 & 2.9742 - j1.8344 \end{bmatrix}. \quad (20c)$$

In this case, the antenna elements are with the same structure and symmetrical array distribution. Therefore, the decoupling network shown in Fig. 2 can be simplified to a symmetrical configuration, where $\theta_{1\alpha} = \theta_{1\beta} = \theta_1$, and $\theta_{3\alpha} = \theta_{3\beta} = \theta_{3\gamma} = \theta_{3\delta} = \theta_3$, $\theta_{4\alpha} = \theta_{4\beta} = \theta_4$. Consequently, (5) can be written as

$$\tan\theta_1 = \frac{-\mathrm{Im}[A_{41} + D_{41}] \pm \sqrt{\mathrm{Im}^2[A_{41} + D_{41}] + 4\mathrm{Re}[B_{41}]\mathrm{Re}[C_{41}]}}{2\mathrm{Re}[C_{41}]Z_1}. \quad (21)$$

If Z_1 is set as a free variable, there always has a solution for θ_1 under the requirement of a non-negative determinant

$$\mathrm{Im}^2[A_{41} + D_{41}] + 4\mathrm{Re}[B_{41}]\mathrm{Re}[C_{41}] \geq 0. \quad (22)$$

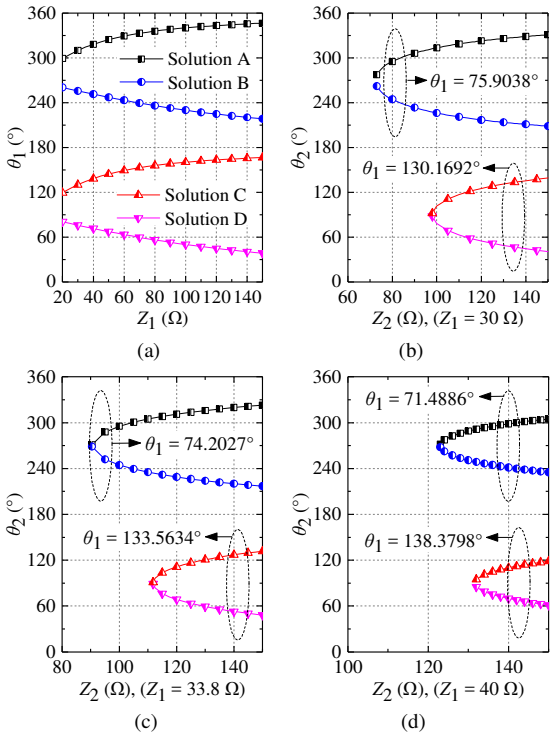

Fig. 9. Graphical formulations of the proposed decoupling network under some specified values of parameters. (a) θ_1 versus Z_1. (b) θ_2 versus Z_2 when $Z_1 = 30$ Ω. (c) θ_2 versus Z_2 when $Z_1 = 33.8$ Ω. (d) θ_2 versus Z_2 when $Z_1 = 40$

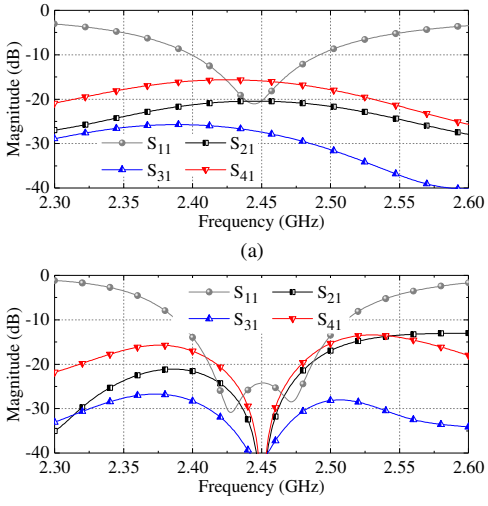

Fig. 10. (a) Simulated transmission responses of the 2×2 antenna array without decoupling. (b) Calculated transmission responses with the proposed decoupling method.

In this case, it can be easily verified that the values provided in (20c) satisfy the requirement expressed in (22). Next, based on the analyses and discussions carried out in Section II, graphical studies are performed to show the determinations of the parameters. For a given Z_1, the value of θ_1 is estimated from (20) and (21), as plotted in Fig. 9(a). It is seen that there are four solutions for θ_1 within the range of 0-360° with a specified Z_1. Subsequently, Z_2 and θ_2 are obtained by using (6) with selected Z_1 and θ_1, and part of the results are graphically depicted in Figs. 9(b)-9(d). One can see that a smaller value of Z_1 leads to a larger acceptable range for Z_2, which is similar for θ_2. From

This article has been accepted for publication in a future issue of this journal, but has not been fully edited. Content may change prior to final publication. Citation information: DOI 10.1109/TAP.2019.2900406, IEEE Transactions on Antennas and Propagation

these results, it is easy to find a group of Z_1, θ_1, Z_2, and θ_2 under the requirement of (12) by using a circuit simulator (ADS in this work) with proper algorithm. Further, the rest parameters (Z_3, $\theta_{3\alpha}$, $\theta_{3\beta}$, $\theta_{3\gamma}$, $\theta_{3\delta}$, Z_4, $\theta_{4\alpha}$, $\theta_{4\beta}$) can be determined based on (12)-(16) and (20). An effective group of the values is: θ_1 = 74.2°, θ_2 = 314.6°, $\theta_{3\alpha} = \theta_{3\beta} = \theta_{3\gamma} = \theta_{3\delta}$ = 193.5°, $\theta_{4\alpha} = \theta_{4\beta}$ = 106.8°, Z_1 =33.8 Ω, Z_2 =126.6 Ω, Z_3 =109.7 Ω, Z_4 =136.7 Ω. Fig. 10 shows the calculated transmission responses among ports 1-4 for the antenna array without/with the proposed decoupling method using the group of the values. Here, multisection transformers are employed as the matching networks, which will be detailed in the next part. It is observed that the magnitudes of original couplings between port 1 and the other three ports are respectively −20.5 dB, −27.4 dB, and −15.9 dB at 2.45 GHz, which are well canceled after combining with the decoupling network using numerical calculations.

B. *Determination of the layout*

TABLE I THEORETICAL VALUES OF THE PARAMETERS

Components	Parameters	VP[1] (Ω / degree)	HP[2] (Ω / degree)
TL_1, TL_4	Z_1 / $\theta_{1\alpha}$	33.8 / 74.2	34.1 / 238.9
TL_2, TL_5	Z_1 / $\theta_{1\beta}$		
TL_3, TL_6	Z_2 / θ_2	126.6 / 314.6	135.1 / 310.8
TL_7	Z_3 / $\theta_{3\alpha}$	109.7 / 193.5	35.1 / 400.3
TL_8	Z_3 / $\theta_{3\beta}$		
TL_{10}	Z_3 / $\theta_{3\gamma}$		
TL_{11}	Z_3 / $\theta_{3\delta}$		
TL_9	Z_4 / $\theta_{4\alpha}$	136.7 / 106.8	134.9 / 396.4
TL_{12}	Z_4 / $\theta_{4\beta}$		
TL_{13}	Z_{m1} / θ_{m1}	62.9 / 73.1	51.7 / 18.8
TL_{14}	Z_{m2} / θ_{m2}	94.3 / 46.8	39.4 / 62.1
TL_{15}	Z_{m3} / θ_{m3}	122.3 / 42.8	93.9 /66.1
TL_{16}	Z_{16} / θ_{16}	57.3 / 43.3	–
TL_{17}	Z_{17} / θ_{17}	50.0 / 49.7	–

[1] Corresponds to the network for the ports 1-4 with vertical polarization.
[2] Corresponds to the network for the ports 5-8 with horizontal polarization.

The numerical studies discussed above describe the design description of the decoupling network for ports 1-4, and provide a group of values of the parameters, whose availability has been numerically verified as shown in Fig. 10. As for the decoupling among the ports 5-8, similar studies can be employed to obtain the theoretical values of the parameters, thus are not detailed for brevity. Eventually, combining the two developed networks together in a single layer, the decoupling for the 2×2 dual-polarized antenna array is achieved. An effective group of the values is listed in Table I.

The layout of the combined decoupling network is then constructed, as shown in Fig. 11. The combined network is printed on a single Rogers RO3003 substrate (ε_r = 3, tanδ = 0.001) with the thickness of 0.762 mm. Multisection transformers are employed for final impedance matching, as illustrated in Fig. 11(b). In addition, extra feeding structures are introduced for ports 1-4. The configuration of the structure is shown in Fig. 11(c), consisting of a soldering pad with a radius of R = 4 mm, a 50-Ω transmission line (TL_{17}) and two open stubs (TL_{16}). Considering that the combined decoupling network is realized in a single layer, the electric lengths of some transmission lines are determined properly over 360° owing to the limited spaces for distributions, as shown in Table I. Converting all ideal parameters to physical values with finely tunings using full-wave simulations, the layout of the decoupling network can be finally determined. The full-wave simulated results will be presented in the next section along with the measured results.

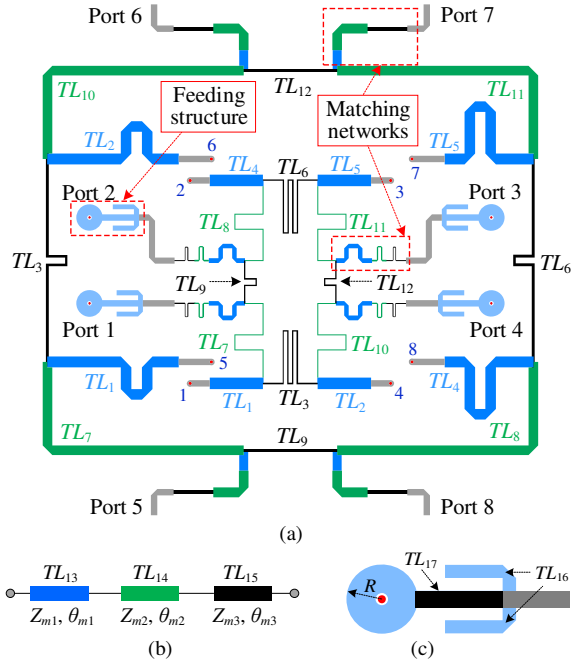

Fig. 11. (a) Layout of the proposed decoupling network for the 2×2 dual-polarized antenna array. Configurations of (b) the matching network using the classical multi-section transformer and (c) the feeding structure.

IV. FULL-WAVE SIMULATION AND MEASUREMENT

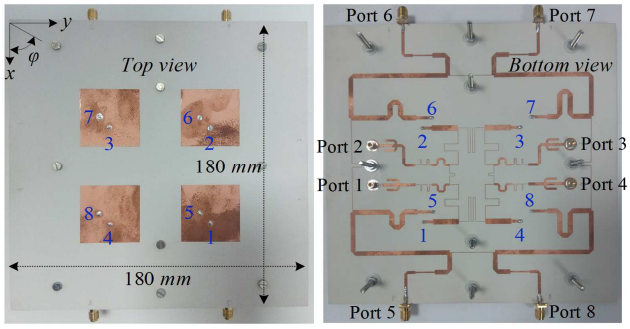

Fig. 12. Photographs of the developed 2×2 dual-polarized antenna array integrated with the proposed decoupling network.

The developed antenna array integrated with the designed decoupling network shown in Fig. 11 is fabricated, and assembled, as photographed in Fig. 12. The overall size of the prototype is 180×180×5.524 mm^3. Several metal screws are utilized for fixation. The prototype is fully tested. The S-parameters and radiation characteristics are measured by using the Agilent 85309B network analyzer and the in-house SATIMO SG24L spherical near-field scanner, respectively.

This article has been accepted for publication in a future issue of this journal, but has not been fully edited. Content may change prior to final publication. Citation information: DOI 10.1109/TAP.2019.2900406, IEEE Transactions on Antennas and Propagation

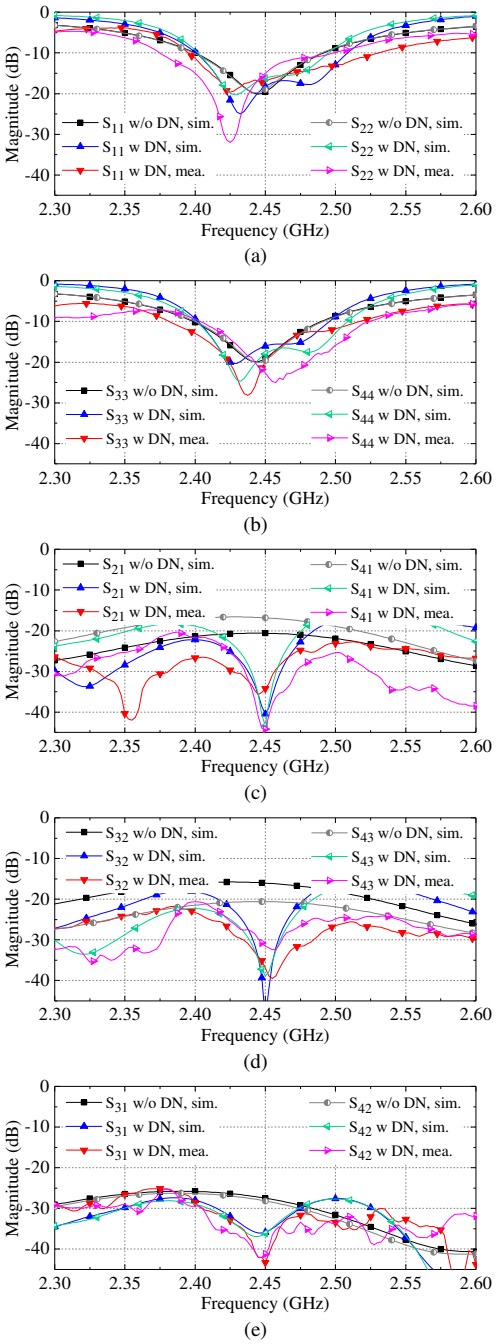

Fig. 13. Measured and simulated S-parameters of the developed prototype for the ports 1-4 with vertical polarization. (a) S_{11} and S_{22}. (b) S_{33} and S_{44}. (c) S_{21} and S_{41}. (d) S_{32} and S_{42}. (e) S_{31} and S_{42}.

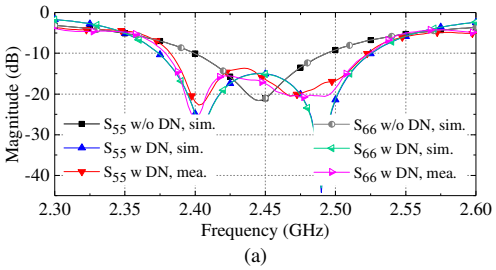

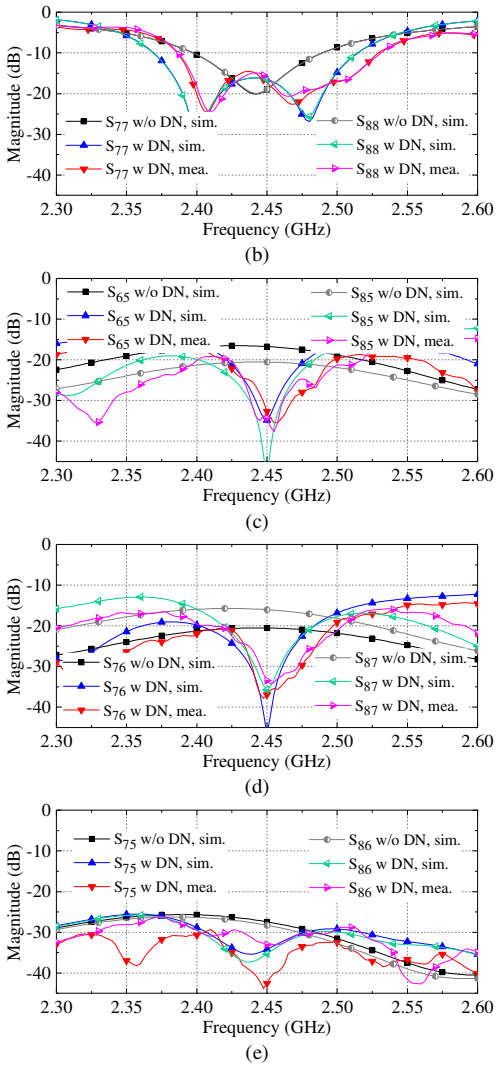

Fig. 14. Measured and simulated S-parameters of the developed prototype for the ports 5-8 with horizontal polarization. (a) S_{55} and S_{66}. (b) S_{77} and S_{88}. (c) S_{65} and S_{85}. (d) S_{76} and S_{87}. (e) S_{75} and S_{86}.

Fig. 13 illustrates the measured S-parameters of ports 1-4, along with the simulated results with and without using the proposed decoupling method. It is seen that the measured results are consistent with the simulated results. Referring to the return loss of higher than 10 dB, the impedance bandwidths of all the eight ports are increased after decoupling compared to the simulations without decoupling, from less than 95 MHz to over 125 MHz. Significant improvement in port isolation corresponding to the co-polarization is achieved. At the center frequency of 2.45 GHz, the isolations are higher than 32 dB after decoupling. For instance, the coupling between two adjacent elements at the vertical orientation, i.e., S_{21}, is reduced from about −21 to −35 dB. For that of the horizontal pairs, S_{41}, is decreased from −16 to below −40 dB. Furthermore, the leakages between the diagonal pairs, S_{31} and S_{42}, are also suppressed to less than −40 dB. As for the ports 5-8, similar results are observed as shown in Fig. 14, and thus are not detailed here for brevity. Note that despite the accordance between the measured and simulated results, the impedance bandwidth of the ports 5-8 is wider than that of the ports 1-4.

This article has been accepted for publication in a future issue of this journal, but has not been fully edited. Content may change prior to final publication. Citation information: DOI 10.1109/TAP.2019.2900406, IEEE Transactions on Antennas and Propagation

This is mainly due to the additional feeding structure for the ports 1-4 as given in Fig. 11(c) that influences the impedance characteristics slightly. Fig. 15 plots the transmission responses between the ports with cross-polarization. Here, results between port 1 and ports 5-8 are given. It is clearly seen that the proposed decoupling network has little influence on the coupling within cross-polarization, where the measured isolations are still better than 30 dB at the center frequency. This also reveals that although meandered lines are utilized for compactness purpose leading to a small space between several transmission lines, the effect of the coupling among these lines on the isolation performance is slight and can be ignored.

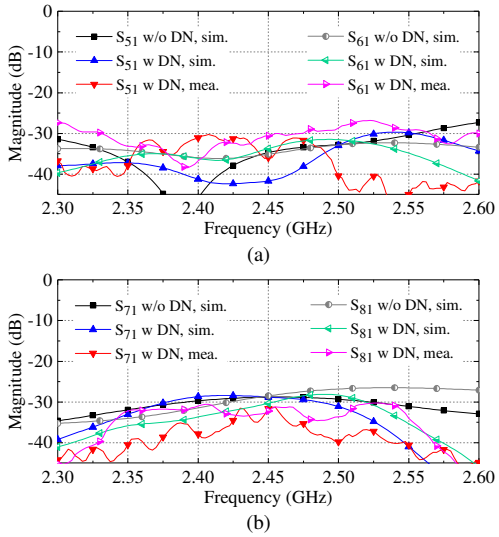

Fig. 15. Measured and simulated transmission responses between port 1 and ports 5-8. (a) S_{51} and S_{61}. (b) S_{71} and S_{81}.

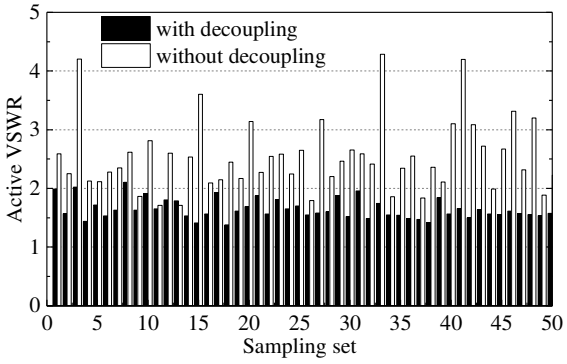

Fig. 16. Worst active reflection coefficients among the eight ports of the dual-polarized 2×2 array, using the same settings reported in [26].

As mentioned in Section I that the active impedance matching of antenna elements would be dramatically affected by the coupling level among the elements. Here, in order to verify the practical improvement of the proposed decoupling method to the 2×2 dual-polarized MIMO array, the active reflection coefficients of the antenna elements are calculated by using the zero-forcing precoding scheme [28]. As shown in Fig. 16, the active VSWR denotes that the impedance matching performance is worsened without decoupling, which would be significantly decreased to less than two for nearly all the 50 random sets of weighting coefficients with the proposed decoupling network.

The measured radiation patterns of some representative elements are shown in Fig. 17. One can find that excellent correlation is observed between the measurements and the simulated results for both with and without the presented decoupling method. This is the same for the other elements, which is not provided for brevity. Some cross-polarization levels are a little high, such as the one shown in Fig. 17(d). This is due to the asymmetrical boundary of the antenna elements and the limited size of the ground plane, but not the decoupling method. It means the proposed network will not change the radiation performance, which is an important feature for phased arrays or massive MIMO arrays. Besides, the total efficiency of the decoupled antenna array with different excitation ports (unexcited ports were terminated with 50-Ω loads) is measured, as depicted in Fig. 18. The simulated results without decoupling are also plotted. The measured total efficiency is found to be higher than 84% for all the eight ports, and are slightly higher with some fluctuations compared to the simulated results before decoupling. This may be probably due to the measurement precision of the chamber. The realized gains at the boresight are around 5.3 dBi after decoupling, which are close to those without decoupling.

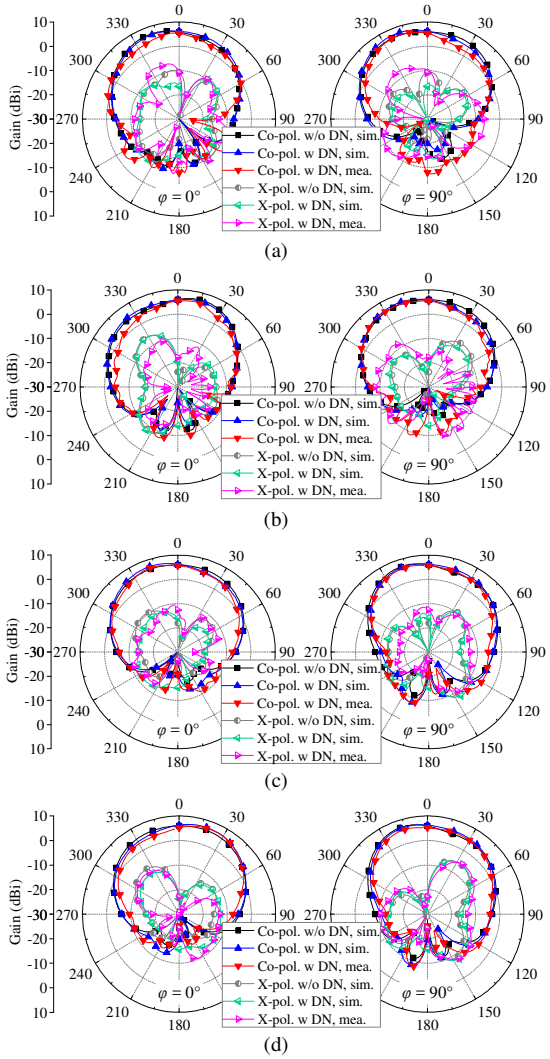

Fig. 17. Measured and simulated radiation patterns of some representative ports. (a) Port 1. (b) Port 2. (c) Port 5. (d) Port 6.

This article has been accepted for publication in a future issue of this journal, but has not been fully edited. Content may change prior to final publication. Citation information: DOI 10.1109/TAP.2019.2900406, IEEE Transactions on Antennas and Propagation

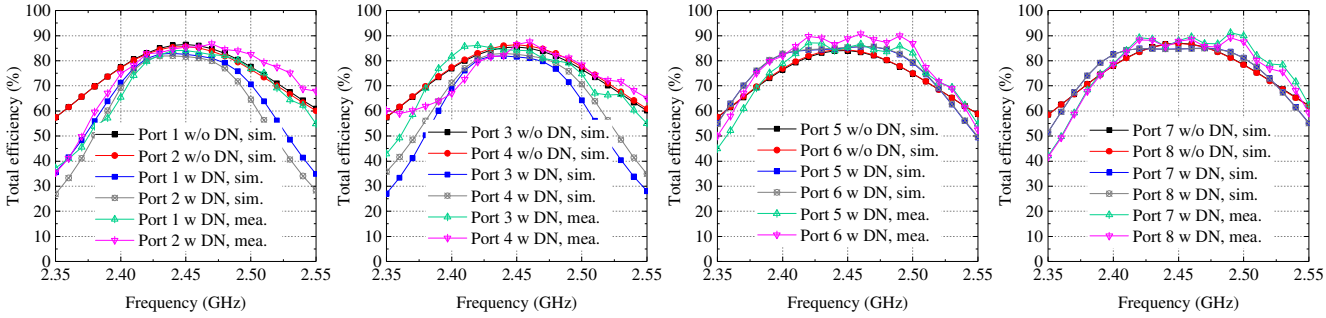

(a) (b) (c) (d)

Fig. 18. Measured and simulated total efficiencies. (a) Ports 1, 2. (b) Ports 3, 4. (c) Ports 5, 6. (d) Ports 7, 8.

TABLE II
PERFORMANCE COMPARISONS AMONG SOME PUBLISHED AND THE PROPOSED DECOUPLING METHODS

Ref./Year	[12]/2017	[19]/2015	[20]/2017	[23]/2008	[24]/2014	**This work**
Decoupling method & center frequency	*LC* circuit @0.74 GHz	Transmission line @7.7 GHz	Transmission line @2.6 GHz	Transmission line @2.6 GHz	Dummy array @2.6 GHz	Transmission line @2.45 GHz
Antenna type	Monopole	Microstrip patch	Monopole	Monopole	Monopole	Microstrip patch
Antenna polarization	Single-polarization	Single-polarization	Single-polarization	Single-polarization	Single-polarization	Dual-polarization
Array configuration	1×2	1×16	1×3	2×2	2×2	2×2
Center distance among adjacent elements	< $0.24\lambda_0$	$0.5\lambda_0$	$0.25\lambda_0$	$0.17\lambda_0$	$0.21\lambda_0$	$0.5\lambda_0$
Isolation between elements with co-polarization	> 20 dB	> 30 dB	> 27.5 dB	> 20 dB	20~27 dB	> 30 dB
Isolation between elements with cross-polarization	–	–	–	–	–	> 30 dB
Total efficiency	> 67%	–	–	–	> 85%	> 84%
Effective for large scale dual-polarized arrays	–	–	–	–	–	Yes

For comparison purpose, some recently published decoupling methods are summarized, as listed in Table II. All of these studies are just attractive for linear arrays or arrays with single polarization. On the other hand, it has been demonstrated that the proposed decoupling method can deal with 2×2 dual-polarized antenna arrays, resulting in well-canceled coupling among the co-polarized antenna elements. Meanwhile, the isolation performance between orthogonal polarizations is not degraded, which maintains a high level of over 30 dB. Since only distributed components featuring low loss and low cost are employed in the presented network, the total efficiency is over 84%, exhibiting well-designed transmission and radiation responses where the correlation coefficients are lower than 0.1 within the impedance band. Please note that the isolation does not feature a wide band response, since the bandwidth is determined by both the performance of the transmission lines and the coupling among the antenna elements. For the developed demonstrator, the wider the impedance bandwidth of the patch antenna element is, the wider the isolation bandwidth would be. On the other hand, due to the limited band response of the transmission lines, we believe that for the antenna with a relatively wide band such as the monopole, the decoupling bandwidth would be narrower than its impedance bandwidth by using the proposed method. This can also be observed from some published works using transmission-line-based decoupling network for small arrays [20], [23]. Moreover, the couplings among large-scale arrays can be suppressed by extending the proposed scheme plotted in Fig. 2 to a lattice configuration. The analysis and design procedure presented in Section II are still effective for the decoupling of the large-scale arrays, but the parameter values of the transmission lines should be different from those for the 2×2 arrays due to the different environments. This is of great significance for the applications of phased arrays and massive MIMO arrays, which will be detailed and discussed in the next section.

V. DECOUPLING NETWORK FOR LARGE-SCALE ARRAYS

In this section, a decoupling network for large-scale MIMO arrays is proposed based on the presented scheme. As plotted in Fig. 19(a), a decoupling network for M×N arrays is given. The antenna elements are marked as A_1 to $A_{M\times N}$, and the corresponding ports are P_1 to $P_{M\times N}$. Please note that the proposed scheme focuses on the decoupling between the adjacent elements, such as A_1 and A_2, A_1 and A_{N+1}, A_1 and A_{N+2}. We believe that the unmentioned couplings (the couplings among the non-adjacent elements, and the ones between the elements with cross-polarization) are weak enough and can be ignored. Thus, there are no suppression techniques for the unmentioned coupling.

This article has been accepted for publication in a future issue of this journal, but has not been fully edited. Content may change prior to final publication. Citation information: DOI 10.1109/TAP.2019.2900406, IEEE Transactions on Antennas and Propagation

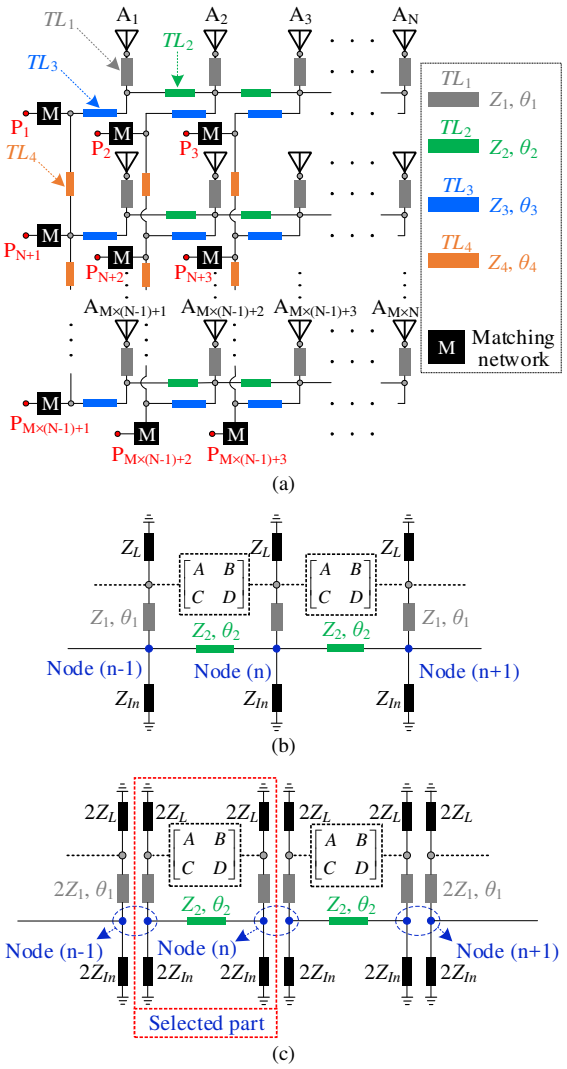

Fig. 19. (a) Block diagram of the proposed decoupling network for M×N MIMO arrays. (b) Equivalent model between three adjacent antenna elements. (c) Simplified circuit of the model provided in Fig. 19(b) in symmetric form.

Fig. 19(b) shows the equivalent model between three horizontally adjacent antenna elements (A_{n-1}, A_n, A_{n+1}) based on the scheme plotted in Fig. 19(a). [*A B*; *C D*] is the transmission matrix of the coupling between two adjacent elements. Z_L and Z_{In} are the equivalent loads of the antenna element and the source, respectively. Owing to the symmetry, the equivalent model can be further simplified, as illustrated in Fig. 19(c). It is found from Fig. 19(c) that the selected part in the red block is the decoupling network for elements A_{n-1} and A_n, which is identical with the one shown in Fig. 3. For the diagonal and vertical pairs in the large antenna array, similar circuits can be constructed corresponding to the ones shown in Fig. 4 and Fig. 5, which is not provided for brevity. According to the above discussions, it is clearly seen that the decoupling method proposed in Section II can be utilized to verify the decoupling performance of the network for large-scale arrays. All the parameter values of the transmission lines can be determined by following the three steps as discussed in Section II-A, II-B, and II-C. More detailed, the decoupling for each row of the elements (such as A_1 to A_N) is firstly operated, and then the decoupling for the adjacently diagonal pairs (such as A_1 and A_{N+2}, A_2 and A_{N+1}) is subsequently achieved, and finally the decoupling for each column (such as A_1 and A_{N+1}, A_2 and A_{N+2}) is realized. The matching network is positioned at the interface of every output. By following the design procedure discussed in (1)-(16), (21) and (22), the parameters of the transmission lines (TL_1, TL_2, TL_3, and TL_4) shown in Fig. 19 can be determined. It should be noted that the values of the parameters for large-scale arrays should not equal to those for the 2×2 array shown in Fig. 2, since the equivalent loads of the antenna element and source are different. Furthermore, the discussions from Fig. 19(c) imply that the signal flowing between adjacent nodes through the decoupling network would be canceled. For instance, the signal leaking from node (n-1) to node (n) through the transmission-line bridge would be canceled with the one through the coupling between elements A_{n-1} and A_n. Hence, there would be no signal transmitted from node (n-1) to node (n+1) through the decoupling network. This denotes that the isolation between the non-adjacent elements would not be affected by the proposed decoupling scheme. Consequently, by employing the proposed design procedure to construct two independent decoupling networks for the two subarrays with cross-polarization, a decoupling network for dual-polarized M×N MIMO arrays can be realized.

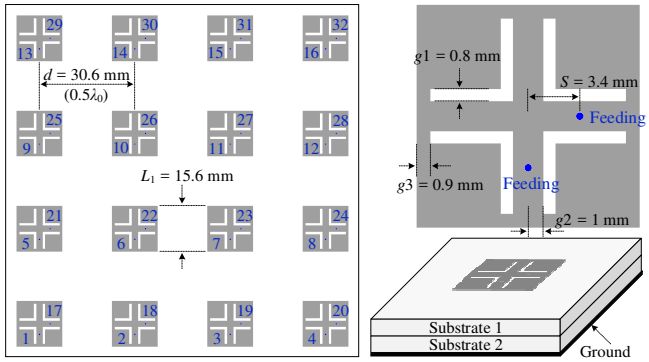

Fig. 20. Configuration of the dual-polarized 2×8 patch array. Rogers RO4350B substrate is used for substrate 1, with the relative permittivity and thickness of 3.66 and 0.762 mm respectively, which are 2.2 and 3 mm correspondingly for substrate 2.

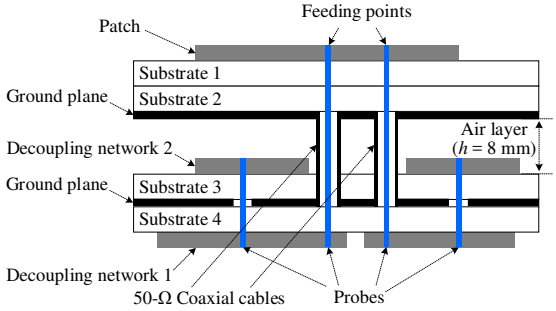

Fig. 21. Side-view of a single dual-polarized element in the 4×4 array with decoupling network, where substrates 3 and 4 are the Rogers RO4350B substrate with the relative permittivity and thickness of 3.66 and 0.762 mm, respectively.

For demonstration purpose, a design example of a 4×4 dual-polarized patch array is provided to show the decoupling performance of the proposed scheme. The proposed method can be easily scaled to the dual-polarized array with a larger

This article has been accepted for publication in a future issue of this journal, but has not been fully edited. Content may change prior to final publication. Citation information: DOI 10.1109/TAP.2019.2900406, IEEE Transactions on Antennas and Propagation

number of antenna elements. Fig. 20 illustrates the array configuration, where the ports with vertical and horizontal polarization are marked as ports 1 to 16 and ports 17 to 32, respectively. Dual-polarized patch antennas centered at 4.9 GHz are employed as the array elements. The L-slots on the patches are used to enhance the isolation between the two ports within a single element. The side view of the 4×4 array integrated with the proposed decoupling network is illustrated in Fig. 21. Two additional layers (substrates 3 and 4) are introduced for realizing the decoupling network. Through the 50-Ω coaxial cables, the patches are directly connected to decoupling network 1 positioned on the bottom of substrate 4, which corresponds to the first two decoupling steps. The third decoupling step (corresponding to decoupling network 2) is operated on the top of substrate 3 along with the matching network.

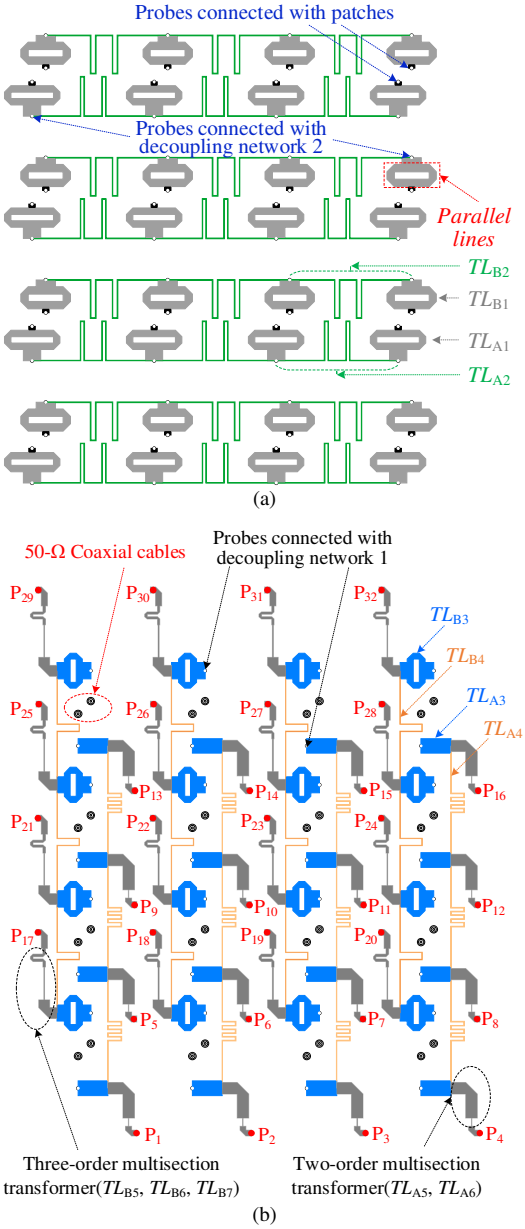

Fig. 22. Layouts of (a) the decoupling network 1 and (b) the decoupling network 2.

Following the design procedure discussed in Section II and Section III, the theoretical values of the transmission lines marked in Fig. 19 can be determined, as listed in Table III. The layout of the decoupling network is shown in Fig. 22. Note that some pairs of parallel lines are utilized. For example, the pair marked in Fig. 22(a) represents a transmission line with the electric length and characteristic impedance of θ_{B1} and Z_{B1} respectively, which is realized by using two parallel lines with the electric length and characteristic impedance of θ_{B1} and $2Z_{B1}$. Using this implementation is for compactness purpose since a transmission line featuring a higher characteristic impedance would have a narrower physical width. Additionally, there is no restriction on the thickness of the air layer shown in Fig. 21, which can be removed by using low-profile techniques such as the multilayer PCB technique. For the ports representing the vertical polarization and horizontal polarization, two- and three-order multi-section transformers are employed for impedance matching respectively. This is similar to the technique shown in Fig. 11(b).

TABLE III THEORETICAL VALUES OF THE PARAMETERS

Components	Z/θ(Ω / degree)	Components	Z/θ(Ω / degree)
TL_{A1}	25.0 / 138.7	TL_{B1}	23.0 / 115.4
TL_{A2}	134.0 / 282	TL_{B2}	133.0 / 280.0
TL_{A3}	27.0 / 76.6	TL_{B3}	25.0 / 141.8
TL_{A4}	126.6 / 450.4	TL_{B4}	139.1 / 313.0
TL_{A5}	32.3 / 132.1	TL_{B5}	33.8 / 70.0
TL_{A6}	140.5 / 13.6	TL_{B6}	119.3 / 81.1
–	–	TL_{B7}	80.2 / 98.1

Next, full-wave simulations of the developed 4×4 array are carried out. For the 3D model, most of the situations encountered by the actual implementation have been taken into account, including the realizations of the antennas and feeding points, the transitions between different layers as well as the couplings among transmission lines. Here, the dual-polarized element corresponding to ports 6 and 22 is chosen as the representative case, since this element exhibits the most complicated coupling response. Fig. 23 shows the simulated transmission responses between some representative ports with/without the decoupling network. It is found from Figs. 23(a)-23(c) that the isolations between the adjacent elements with co-polarization are improved to over 28 dB with the decoupling network at the center frequency. Meanwhile, the worst isolation between the non-adjacent ones with co-polarization, $S_{8,6}$, is still higher than 24.3 dB as given in Fig. 23(d). The isolations between some cross-polarized ports are also provided as shown in Fig. 23(e), which are still better than 28.5 dB after decoupling. This implies that nearly no degradation in the isolation is realized by using the proposed decoupling network. As for the unmentioned mutual couplings, similar improvements or results are observed and thus are not detailed here. For the radiation performance, good accordance between the results with/without decoupling is observed. The results are similar to those plotted in Fig. 16, and not provided for brevity. The total efficiency of the antenna elements at the center frequency with and without decoupling are among

This article has been accepted for publication in a future issue of this journal, but has not been fully edited. Content may change prior to final publication. Citation information: DOI 10.1109/TAP.2019.2900406, IEEE Transactions on Antennas and Propagation

70%-82% and 75%-86%, respectively. The decoupled total efficiency of port 17 is with the worst deterioration of 9.5%, but still higher than 75%. Here, the worst deterioration of the total efficiency represents a small insertion loss of around 0.45 dB, which would not increase the cost of the entire system significantly. Summarily, based on the above studies, it can be verified that the proposed scheme characterizes well-designed isolation improvement, low insertion loss, and is of great attraction for phased array and massive MIMO array systems.

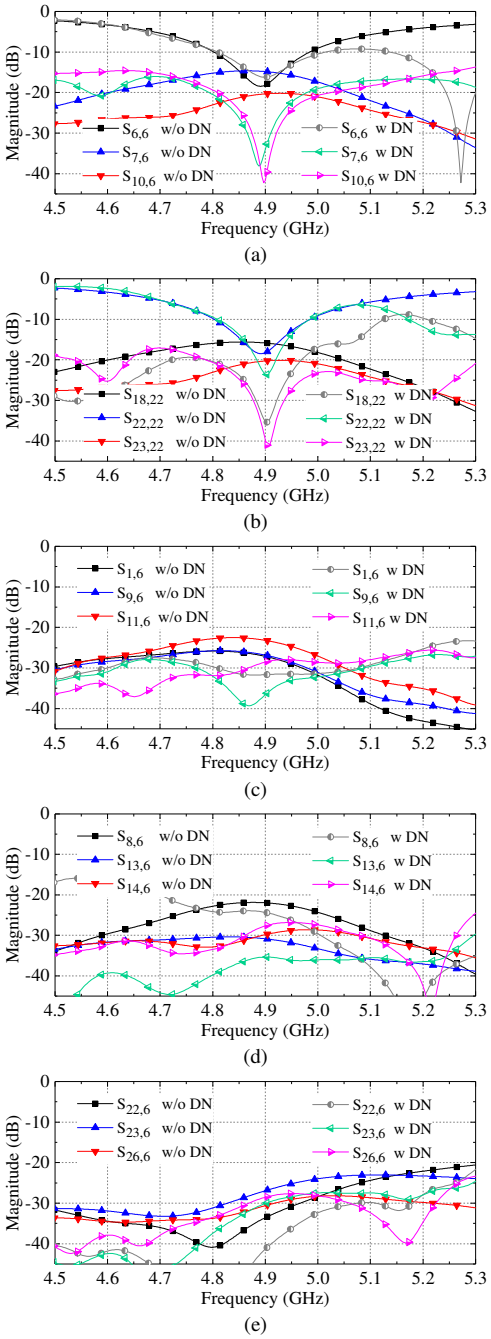

Fig. 23. Full-wave simulated S-parameters of the developed 4×4 array. (a) $S_{6,6}$, $S_{7,6}$ and $S_{10,6}$. (b) $S_{18,22}$, $S_{22,22}$ and $S_{23,22}$. (c) $S_{1,6}$, $S_{9,6}$ and $S_{11,6}$. (d) $S_{8,6}$, $S_{13,6}$ and $S_{14,6}$. (e) $S_{22,6}$, $S_{23,6}$ and $S_{26,6}$.

VI. Conclusion

This study presents a compact and low-profile decoupling approach to suppress the mutual coupling within 2×2 and large-scale dual-polarized MIMO antenna arrays. By using the proposed architecture, the coupling between the adjacent elements with co-polarization can be well canceled theoretically, with almost no degradation in the isolation performance between the ports corresponding to cross-polarization and non-adjacent elements. The proposed scheme features low insertion loss and facilitates highly integrated implementations for practical designs. Two demonstrators for 2×2 and 4×4 dual-polarized arrays are developed, respectively. Theoretical calculations, full-wave simulations, and measurements have been carried out for verification purposes. It is expected that the proposed decoupling method can be widely utilized for phased array and massive MIMO array systems.

Appendix: Derivation of (5), (6), and (21)

As discussed in Section II, the results shown in (5) and (6) are obtained based on (1)-(4). The detailed derivations are given as follows. Firstly, substituting (3a) into (4), we have

$$b_1 + b_2 = F_{41} = 0 \tag{23}$$

Subsequently, using (3b) and (3c) in (23), we get

$$\begin{aligned} F_{41} = {} & jA_{41}Z_1\cos\theta_{1\alpha}\sin\theta_{1\beta} + jD_{41}Z_1\sin\theta_{1\alpha}\cos\theta_{1\beta} + B_{41}\cos\theta_{1\alpha}\cos\theta_{1\beta} \\ & - C_{41}Z_1^2\sin\theta_{1\alpha}\sin\theta_{1\beta} + jZ_1\sin\theta_2 = 0 \end{aligned} \tag{24}$$

The real part of the parameter F_{41} is

$$\begin{aligned} \mathrm{Re}[F_{41}] = {} & -\mathrm{Im}[A_{41}]Z_1\cos\theta_{1\alpha}\sin\theta_{1\beta} - \mathrm{Im}[D_{41}]Z_1\sin\theta_{1\alpha}\cos\theta_{1\beta} \\ & + \mathrm{Re}[B_{41}]\cos\theta_{1\alpha}\cos\theta_{1\beta} - \mathrm{Re}[C_{41}]Z_1^2\sin\theta_{1\alpha}\sin\theta_{1\beta} = 0 \end{aligned} \tag{25}$$

Based on (25), we have

$$\begin{aligned} \frac{\mathrm{Re}[F_{41}]}{\cos\theta_{1\alpha}\cos\theta_{1\beta}} = {} & -\mathrm{Im}[A_{41}]Z_1\tan\theta_{1\beta} - \mathrm{Im}[D_{41}]Z_1\tan\theta_{1\alpha} \\ & + \mathrm{Re}[B_{41}] - \mathrm{Re}[C_{41}]Z_1^2\tan\theta_{1\alpha}\tan\theta_{1\beta} = 0 \end{aligned} \tag{26}$$

From (26), the result expressed in (5) can be directly obtained. On the other hand, based on (3a), (3c) and (4), we have

$$\frac{1}{b_1} + \frac{1}{b_2} = \frac{1}{b_1} + \frac{1}{jZ_1\sin\theta_2} = 0 \tag{27}$$

Further,

$$\mathrm{Im}\left[\frac{1}{b_1}\right] + \mathrm{Im}\left[\frac{1}{jZ_1\sin\theta_2}\right] = \mathrm{Re}\left[\frac{1}{b_1}\right] + \mathrm{Re}\left[\frac{1}{jZ_1\sin\theta_2}\right] = 0 \tag{28}$$

Based on (28), the numerical relation shown in (6) is derived. According to the condition that $\theta_{1\alpha} = \theta_{1\beta} = \theta_1$, (26) can be simplified as

$$\begin{aligned} \frac{\mathrm{Re}[F_{41}]}{\cos^2\theta_1} = {} & -\mathrm{Im}[A_{41}]Z_1\tan\theta_1 - \mathrm{Im}[D_{41}]Z_1\tan\theta_1 \\ & + \mathrm{Re}[B_{41}] - \mathrm{Re}[C_{41}]Z_1^2\tan^2\theta_1 = 0 \end{aligned} \tag{29}$$

Then, we have

$$\mathrm{Re}[C_{41}]Z_1^2\tan^2\theta_1 + \mathrm{Im}[A_{41} + D_{41}]Z_1\tan\theta_1 - \mathrm{Re}[B_{41}] = 0 \tag{30}$$

Finally, the result given in (21) can be derived based on the quadratic equation (30).

References

[1] B. Wang, Y. Chang, and Y. Sun, "Performance of the large-scale adaptive array antennas in the presence of mutual coupling," *IEEE Trans. Antennas Propag.*, vol. 64, no. 6, pp. 2236-2245, Jun. 2016.

[2] R. Janaswamy, "Effect of element mutual coupling on the capacity of fixed length linear arrays," *IEEE Antennas Wireless Propag. Lett.,* vol. 1, pp. 157-160, 2002.
[3] D. M. Pozar, "Relation between the active input impedance and the active element pattern of a phased array," *IEEE Trans. Antennas Propag.*, vol. 51, no. 9, pp. 2486-2489, Sep. 2003.
[4] L. Savy and M. Lesturgie, "Coupling effects in MIMO phased array," in *Proc. IEEE Radar Conf.* (*RadarConf*), Philadelphia, PA, USA, May 2016, pp. 1–6.
[5] K.-H. Chen and J.-F. Kiang, "Effect of mutual coupling on the channel capacity of MIMO systems," *IEEE Trans. Veh. Technol.*, vol. 65, no. 1, pp. 398–403, Jan. 2016.
[6] X. Chen, S. Zhang, and Q. Li, "A review of mutual coupling in MIMO systems." *IEEE Access*, vol. 6, pp. 24706-24719, 2018.
[7] C. Fager, X. Bland, K. Hausmair, et al. "Prediction of smart antenna transmitter characteristics using a new behavioral modeling approach," *IEEE MTT-S Int. Microw. Symp.*, Tampa, FL, Jun. 1-6, 2014, pp. 1-4.
[8] L. Yang, M. Fan, F. Chen, J. She, and Z. Feng, "A novel compact electromagnetic-bandgap structure and its applications for microwave circuits," *IEEE Trans. Microw. Theory Tech.*, vol. 53, no. 1, pp. 183-190, Jan. 2005.
[9] I. Dioum, A. Diallo, S. M. Farssi, and C. Luxey, "A novel compact dualband LTE antenna-system for MIMO operation," *IEEE Trans. Antennas Propag.*, vol. 62, no. 4, pp. 2291-2296, Apr. 2014.
[10] C.-H. Wu, C.-L. Chiu, and T.-G. Ma, "Very compact fully lumped decoupling network for a coupled two-element array," *IEEE Antennas Wireless Propag. Lett.,* vol. 15, pp. 158-161, 2016.
[11] H. Makimura, K. Nishimoto, T. Yanagi, T. Fukasawa, and H. Miyashita, "Novel decoupling concept for strongly coupled frequency-dependent antenna arrays," *IEEE Trans. Antennas Propag.*, vol. 65, no. 10, pp. 5147-5154, Oct. 2017.
[12] H. Meng and K.-L. Wu, "An *LC* decoupling network for two antennas working at low frequencies," *IEEE Trans. Microw. Theory Tech.*, vol. 65, no. 7, pp. 2321-2329, Jul. 2017.
[13] K. Qian, L. Zhao, and K.-L. Wu, "An LTCC coupled resonator decoupling network for two antennas," *IEEE Trans. Microw. Theory Tech.*, vol. 63, no. 10, pp. 3199-3207, Oct. 2015.
[14] L. Zhao, L. K. Yeung, and K.-L. Wu, "A coupled resonator decoupling network for two-element compact antenna arrays in mobile terminals," *IEEE Trans. Antennas Propag.*, vol. 62, no. 5, pp. 2767-2776, May 2014.
[15] L. Zhao and K.-L. Wu, "A dual-band coupled resonator decoupling network for two coupled antennas," *IEEE Trans. Antennas Propag.*, vol. 63, no. 7, pp. 2843-2850, Jul. 2015.
[16] K.-C. Lin, C.-H. Wu, C.-H. Lai, and T.-G. Ma, "Novel dual-band decoupling network for two-element closely spaced array using synthesized microstrip lines," *IEEE Trans. Antennas Propag.*, vol. 60, no. 11, pp. 5118-5128, Nov. 2012.
[17] J. Sui and K.-L. Wu, "A general T-stub circuit for decoupling of two dual-band antennas," *IEEE Trans. Microw. Theory Tech.*, vol. 65, no. 6, pp. 2111-2121, Jun. 2017.
[18] Y.-F. Cheng and K.-K. M. Cheng, "A novel dual-band decoupling and matching technique for asymmetric antenna arrays," *IEEE Trans. Microw. Theory Tech.*, vol. 6, no. 5, pp. 2080-2089, May. 2018.
[19] R.-L. Xia, S.-W. Qu, P.-Fa Li, D.-Q. Yang, S. Yang, and Z.-P. Nie, "Wide-angle scanning phased array using an efficient decoupling network," *IEEE Trans. Antennas Propag.*, vol. 63, no. 11, pp. 5161-5165, Nov. 2015.
[20] Y.-F. Cheng and K.-K. M. Cheng, "A novel and simple decoupling method for a three-element antenna array," *IEEE Antennas Wireless Propag. Lett.,* vol. 16, pp. 1072-1075, 2017.
[21] J. Weber, C. Volmer, K. Blau, R. Stephan, and M. A. Hein, "Miniaturized antenna arrays using decoupling networks with realistic elements," *IEEE Trans. Microw. Theory Tech.*, vol. 54, no. 6, pp. 2733-2740, Jun. 2006.
[22] T. Huang, Y. Yu, and L. Yi, "Design of highly isolated compact antenna array for MIMO applications," *Int. J. Antennas Propag.*, vol. 2014, Art. no. 473063, Nov. 2014.
[23] J. C. Coetzee and Y. Yu, "Port decoupling for small arrays by means of an eigenmode feed network," *IEEE Trans. Antennas Propag.*, vol. 56, no. 6, pp. 1587-1593, Jun. 2008.
[24] L. Zhao and K.-L. Wu, "A decoupling technique for four-element symmetric arrays with reactively loaded dummy elements," *IEEE Trans. Antennas Propag.*, vol. 62, no. 8, pp. 4416-4421, Aug. 2014.
[25] Y. Gao, R. Ma, Y. Wang, Q. Zhang, and C. Parini, "Stacked patch antenna with dual-polarization and low mutual coupling for massive MIMO," *IEEE Trans. Antennas Propag.*, vol. 64, no. 10, pp. 4544-4549, Oct. 2016.
[26] K.-L. Wu, C. Wei, X. Mei, and Z.-Y. Zhang, "Array-antenna decoupling surface," *IEEE Trans. Antennas Propag.*, vol. 65, no. 12, pp. 6728-6738, Dec. 2017.
[27] D. M. Pozar, "Chapter 4: Microwave network analysis," in *Microwave Engineering*, 4th ed. John Wiley & Sons, 2012, pp. 188-202.
[28] X. Chen, "Throughput modeling and measurement in an isotropic-scattering reverberation chamber," *IEEE Trans. Antennas Propag.*, vol. 62, no. 4, pp. 2130-2139, Apr. 2014.

Yi-Ming Zhang (S'17) received the B.S. and M.S. degrees from Central China Normal University in 2008 and University of Electronic Science and Technology of China in 2014, respectively. He is now working toward the Ph.D. degree at University of Electronic Science and Technology of China. Since February 2018, he has been a guest researcher with the Antenna, Propagation and Millimeter-wave Systems (APMS) Section, Aalborg University, Denmark. His current research interests include MIMO antenna decoupling, single-channel full-duplex communications, and passive RF and microwave components.

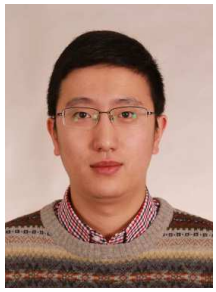

Shuai Zhang (SM'18) received the B.E. degree from the University of Electronic Science and Technology of China, Chengdu, China, in 2007 and the Ph.D. degree in electromagnetic engineering from the Royal Institute of Technology (KTH), Stockholm, Sweden, in 2013. After his Ph.D. studies, he was a Research Fellow at KTH. In April 2014, he joined Aalborg University, Denmark, where he currently works as Associate Professor. In 2010 and 2011, he was a Visiting Researcher at Lund University, Sweden and at Sony Mobile Communications AB, Sweden, respectively. He was also an external antenna specialist at Bang & Olufsen, Denmark from 2016-2017. He has coauthored over 50 articles in well-reputed international journals and over 15 (US or WO) patents. His current research interests include: mobile terminal mmwave antennas, biological effects, CubeSat antennas, Massive MIMO antenna arrays, UWB wind turbine blade deflection sensing, and RFID antennas.

Jia-Lin Li received the M. S. degree from the University of Electronic Science and Technology of China (UESTC), Chengdu, China, in 2004, and the Ph. D. degree from the City University of Hong Kong, Hong Kong, in 2009, both in electronic engineering.

From September 2005 to August 2006, he was a Research Associate with the Wireless Communication Research Center, City University of Hong Kong, Hong Kong. Since September 2009, he has been with the School of Physical Electronics, UESTC, where he is currently a Professor. His research interests include microwave/millimeter-wave antenna and arrays, circuits and systems, interactions between microwave and complex medium, and so on.

Gert Frølund Pedersen was born in 1965. He received the B.Sc. and E.E. (Hons.) degrees in electrical engineering from the College of Technology in Dublin, Dublin Institute of Technology, Dublin, Ireland, in 1991, and the M.Sc.E.E. and Ph.D. degrees from Aalborg University, Aalborg, Denmark, in 1993 and 2003, respectively. Since 1993, he has been with Aalborg University where he is a Full Professor heading the Antennas, Propagation and Millimeter-wave Systems LAB with 25 researchers. He is also the Head of the Doctoral School on wireless communication with some 40 Ph.D. students enrolled. His research interests include radio communication for mobile terminals especially small antennas, diversity systems, propagation, and biological effects. He has published more than 500 peer reviewed papers, 6 books, 12 book chapters and holds over 50

patents. He has also worked as a Consultant for developments of more than 100 antennas for mobile terminals including the first internal antenna for mobile phones in 1994 with lowest SAR, first internal triple-band antenna in 1998 with low SAR and high TRP and TIS, and lately various multiantenna systems rated as the most efficient on the market. He has worked most of the time with joint university and industry projects and have received more than 21 M$ in direct research funding. He is currently the Project Leader of the RANGE project with a total budget of over 8 M$ investigating high performance centimetre/millimetre-wave antennas for 5G mobile phones. He has been one of the pioneers in establishing over-the-air measurement systems. The measurement technique is now well established for mobile terminals with single antennas and he was chairing the various COST groups with liaison to 3GPP and CTIA for over-the-air test of MIMO terminals. He is currently involved in MIMO OTA measurement.